Hindawi
Advances in Civil Engineering
Volume 2018, Article ID 7341523, 10 pages
https://doi.org/10.1155/2018/7341523

Research Article

Experimental Investigation on Permeability and Mechanical Deformation of Coal Containing Gas under Load

Runsheng Lv,[1,2,3] **Bing Li**,[4] **Zhimin Song**,[4] **and Gaofeng Liu**[1]

[1]*School of Resources & Environment, Henan Polytechnic University, Jiaozuo 454003, China*
[2]*School of Civil, Mining and Environmental Engineering, University of Wollongong, Wollongong, New South Wales 2500, Australia*
[3]*Collaborative Innovation Center of Coalbed Methane and Shale Gas for Central Plains Economic Region, 454000 Henan Province, China*
[4]*Henan University of Engineering, Zhengzhou 451191, China*

Correspondence should be addressed to Runsheng Lv; lvrunsheng@hpu.edu.cn

Received 13 August 2018; Accepted 8 October 2018; Published 29 October 2018

Guest Editor: Ray R. Zhang

Coalbed effective permeability is widely used as a primary index to evaluate gas-drainage effect in CBM exploitation field. However, it seems to be difficult to obtain by the reason of dynamic change in close relationship with crustal stress, methane pressure, porosity, and adsorption. Due to their dissimilar adsorption properties and tectonic deformation degrees, different types of coal containing gas have various stress-strain and gas seepage curves. The paper presents the experimental investigations of the dynamic relationship between coal permeability and deformation under load. In this work, stress-strain and permeability investigations were performed using anthracite lump with a vitrinite reflectance of about 3.24% at various pressures and temperatures. The permeability (including the initial, minimum, and maximum) decreased with increasing temperature. At a constant confining pressure, the strains in different directions almost all increased with increasing axial stress and decreased with increasing pore methane pressure during the prefracture stage. At a constant pore pressure, the compression strength of the coal specimens increased approximately linearly during the prefracture stage and sharply decreased during the postfracture stage, while the permeability decreased rapidly and then increased slowly during the prefracture and remained stable during the postfracture stage. The permeability of the coal specimens mainly depended on the inner fissures. The permeability was greater during the postfracture than that during the prefracture stage. At the same temperature, the gas seepage curve of each coal specimen could be divided into three sections: decreasing, increasing, and constant sections. The necessary time for the permeability to reach a steady state increased as the confining and pore pressures increased. At high confining pressures (i.e., 6 MPa and 8 MPa), no significant differences between the methane seepage velocities of the specimens were evident, and their seepage curves were similar to prefracture. However, clear differences were observable at the postfracture stage. The seepage abilities of the coal specimens were more sensitive to stress than temperature in the same condition.

1. Introduction

Coalbed methane predrainage is widely used as an effective method to control coal and gas outburst in underground mine [1]. Coalbed methane (CBM) effective permeability is a key index representing the easy or difficulty degree of methane transportation in CBM exploration and development, which is influenced by many factors, including tectonic stress [2–7], pore pressure [8–10], porosity [11], adsorption deformation [12–16], temperature and pressure (tristress) [8]. Some researchers have conducted permeability experiments using different coal specimens, and a few models of dynamic permeability changes have been established based on the experiment results and theoretical derivations, and these models were widely used to describe the effects of stress and matrix shrinkage/expansion [17–19]. For example, Yin et al. [20] selected outburst and non-outburst molding coal specimens and performed

a permeability experiment at a maximum gas pressure of 1.0 MPa and normal temperature of 30°C. They found that the methane permeability firstly decreased and then slightly increased as increasing confining stress. Wang et al. [15] conducted a sorption-induced swelling/shrinkage and permeability experiment involving CO_2 injection using a specially designed true tristress coal permeameter. Zou et al. [21] experimentally investigated the dependence of coal permeability on effective stress and gas slippage under cyclic loading and discussed the relationship between permeability and effective stress. Coalbeds are a kind of typical unconventional gas reservoirs with matrix and fissure porosities, low permeability, and high sensitivity to effective stress. In the permeability experiment performed by Meng et al. [4], the change relationship between permeability and effective stress has a negative exponential function. When the effective stress was 5 MPa or 6 MPa, the stress sensitivity coefficient and pore compressibility factor fluctuated and decreased gradually, and the permeability damage rate varied slowly. Experimental studies have shown that the overall bituminous coal permeability decreases exponentially with increasing effective stress [2, 22, 23]. However, high-rank anthracite reservoirs have lower permeability and higher adsorption capacities than conventional oil and gas reservoirs [24]. Research on the relationships between in situ stress in coal reservoirs and permeability has been limited or insufficient due to the lack of coal stress-strain and permeability coupling data. Most studies have been based mainly on various rank coal using molding coal specimens that could not represent actual pore structures of a raw coal reservoir. Consequently, understanding of the dynamic permeability variation during CBM exploration and development remains somewhat limited. Therefore, this experimental work on induced swelling strain and permeability under different stress paths is of utmost importance since it will supplement the theoretical studies on CBM exploration and development. The objective of this research was to obtain the effects of varying the strain, pore pressure, and temperature on the permeability of anthracite. Specifically, stress-strain and permeability measurements were performed on anthracite specimens under total stress-strain paths, and the correlations between effective stress, permeability, and stress-strain were analyzed.

2. Experiments

2.1. Specimen Preparation. The large raw block, such as that shown in Figure 1(a), was obtained from a longwall development heading of an underground coal mine currently extracting No. 21 coal seam, Jiaozuo coal basin of northern China. The coal seam No. 21 is located at the bottom of Shanxi formation in the Permian. The maximum vitrinite random reflectivity ($R_{o,max}$) of the coal specimens was 3.24%, and the macroscopic lithotype was semibright to bright coal with banded coal texture. The depth of coal seam No. 21 is 450–480 m. The colliery is experiencing high methane content more than 20 m^3/t in most areas, and gas-drainage results are extremely unsatisfied. Due to strong adsorption of CH_4 and low pore connectedness in the seam, it usually takes longer time to reduce the gas content below the critical value of 8 m^3/t based on China seam outburst regulation. Standard cylindrical specimens of 100 mm in length and 50 mm in diameter were selectively drilled parallel to the stratification plane in the laboratory (Figure 1(b)). It was then burnished using emery cloth of the 100-mesh sieve so that the topside and underside of coal specimens were parallel within 0.1 mm, and the size error between the diameters on topside and underside was less than 0.2 mm. To prevent moisture from influencing the methane adsorption and permeability at different temperatures, all of the experimental specimens were dried in an incubator and then stored in a drying oven until the experiments were performed. The basic data about the coal specimens are provided in Table 1.

2.2. Experimental Apparatus and Procedure. The experimental apparatus was a heat-solid-fluid coupling triaxial servoseepage device on coal containing gas (Figures 2(a) and 2(b)) provided by Key Laboratory of Southwest Resource Development and Environmental Disaster Control Engineering, Education Ministry of China, Chongqing University. To ensure that methane could not enter or exit the experimental device during the permeability tests, a layer of suitable thickness consisting of 704 silica gel was uniformly applied to the circumference of each coal specimen and then dried for 10 hours (Figure 2(c)). Each coal specimen was installed on the specimen platform in the heat-solid-fluid coupling triaxial servoseepage device. Heat-shrink tubing was employed to seal the coal specimen, which was then heated with a heater and the compressor to cause the tubing to cling to the specimen. To ensure the coal sufficient adsorbing gas to reach the equilibrium state, the specimen must be deaerated and the time of deaeration should be no less than 6 hours using a vacuum pump, then the gas cylinder valve was opened, and gas pressure was adjusted to the designed value of the test plan to allow the specimen to adsorb gas for 24 hours. After approaching the methane adsorption equilibrium, the axial and radial displacement extensometer and data acquisition line were installed, as well as the triaxial pressure cell and remaining parts. Axial stress was loaded slowly at a rate of 0.01 kN/s, and gas cylinder and flowmeter valves were then opened to adjust methane pressures at the gas inlet and outlet to designed gas pressure and 0.1 MPa, respectively. The automatic data recording system simultaneously started its operation.

2.3. Experimental Conditions. The cylindrical specimens not exhibiting any visible fractures were selected meticulously to prevent fractures from affecting the permeability and adsorption swelling strain results. In these experiments, CH_4 desorption by inducing the gas pressure is 1 and 2 MPa; the confining pressure was 4, 6, and 8 MPa; and the temperature was 30, 40, and 50°C, respectively. All testing parameters were designed to ensure that the specimen is not broken during entire experimental stages on the base of in situ state.

(a) (b)

Figure 1: (a) Raw coal and (b) cylindrical coal specimen for testing.

Table 1: Features of experimental coal specimens.

Type	Specimen ID	Specimen size (mm)	Weight (g)	Density (g/cm^3)	M_{ad} (%)	A_d (%)	$R_{o,max}$ (%)
Raw coal	W1	Φ49.9 × 100.25	285.1	1.463	0.52	12.45	3.24
	W2	Φ49.9 × 100.68	286.4	1.482	0.55		
	W3	Φ49.9 × 100.88	296.3	1.475	0.50		
	W4	Φ49.9 × 99.90	285.4	1.460	0.55		
	W5	Φ49.9 × 100.05	286.3	1.465	0.53		
	W6	Φ49.9 × 100.00	286.0	1.462	0.54		

M_{ad}: moisture of on air-dry basis; A_d: ash on a dry basis; $R_{o,max}$: maximum reflectivity on vitrinite.

2.4. Permeability Determination. Ideally, a fully adsorption equilibrium state should be reached before commencing permeability testing; however, the methane diffusion process in the tight coal specimen under triaxial stress could be very slow [1, 25], and it was considered that equilibrium was reached after two-day adsorption. As the gas flow rate at the outlet pipeline became stable, the time was about 3 to 4 hours according to the recorded data; using the measured flows, including information about the gas flow rate, gas pressure, specimen stress, and composition of the outlet gas, the permeability of the coal specimen can be calculated using Darcy's law [26]:

$$k = \frac{2qp_1\mu H}{A\left(p_1^2 - p_2^2\right)}, \quad (1)$$

where k is the permeability (mD), q is the volumetric rate of flow (cm^3/s) at the prevailing barometric pressure, μ is the fluid viscosity (cp), H is the specimen length (mm), A is the cross-sectional area of the specimen (mm^2), p_1 is the inlet gas pressure (MPa), and p_2 is the outlet gas pressure (MPa).

3. Results and Discussion

Six specimens were selected to investigate the effects of mechanical deformations on the permeability of high-rank anthracite containing gas in this work. Under a complete stress-strain path, deformation-seepage was only related to whether different coal materials adsorbed gas. All specimens exhibited almost the similar laws of permeability variations with mechanical deformation and temperature change. For simplicity, we discuss only one of the specimens in this report.

3.1. Mechanical Deformation. The relationships between confining pressure, axial stress, and strain direction are depicted in Figure 3. Both triaxial compression strength and strain increase consistently pre- and postfracture as the confining pressure increases from 4 to 6 to 8 MPa. The compression strength increment of the coal specimen increases from 15.3% to 21.7% at a pore pressure of 1 MPa, yet it decreases from 23.7% to 19.7% at a pore pressure of 2 MPa. The coal compression strength is positive correlation to confining pressure at the same external condition, and it becomes larger as increasing confining pressure and more difficult to compress. Because confining pressure restricts coal inner crack to further extend, pores and cracks are compressed to enhance the mutual friction force among coal granules and density before the stress peak of the coal specimen, and the total stress-strain curve appears to vibrate repeatedly in respect to the beginning of coal break.

While gas pressure increasing from 1 to 2 MPa, coal granules may adsorb more methane and bring about larger swelling strain, and it will directly result in smaller pore or crack volume and lower coal strength. Adsorption gas layer can drop the friction force among coal granules as a result of slippage effect.

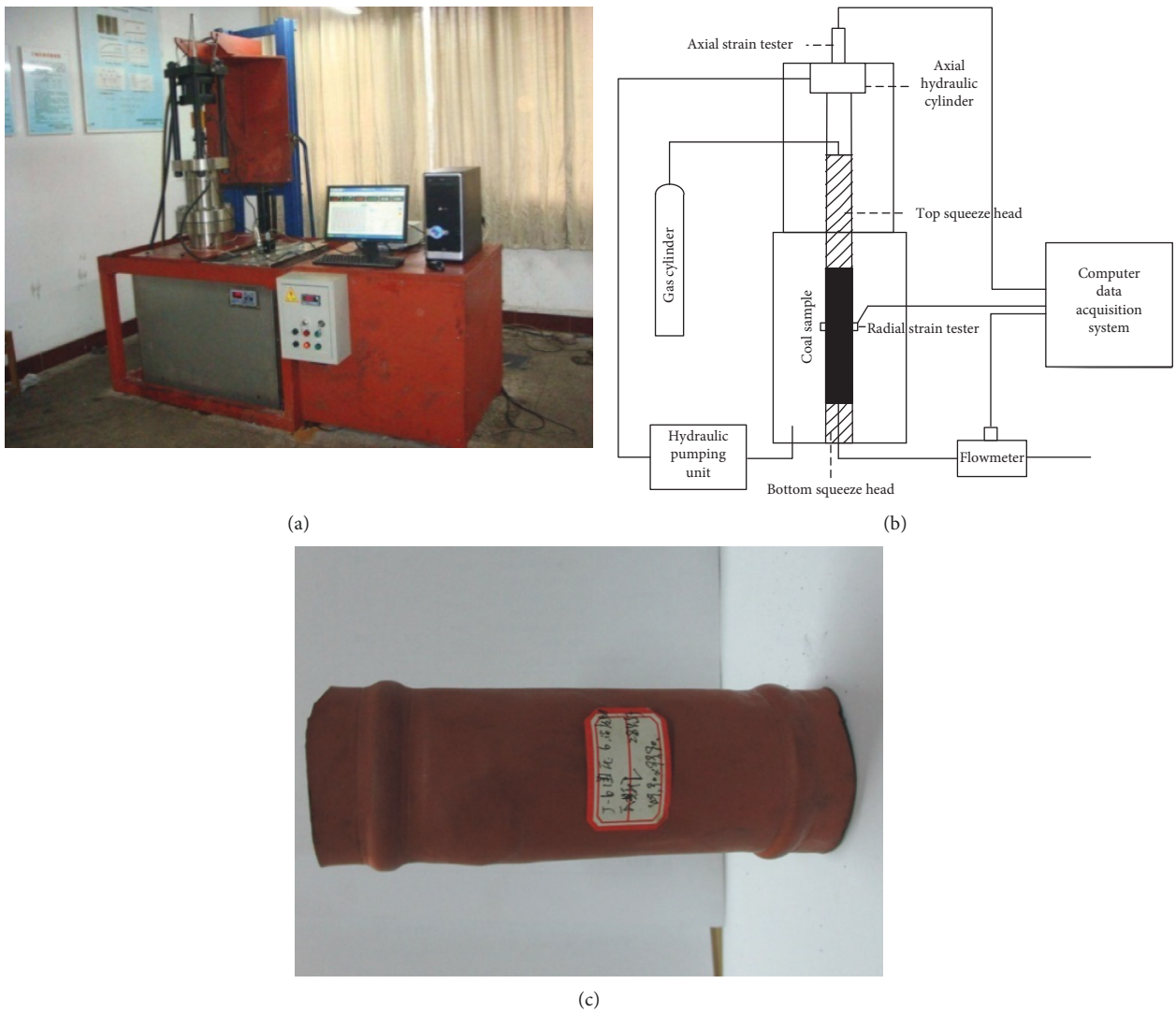

Figure 2: (a) Heat-solid-fluid coupling triaxial seepage device, (b) experimental workflow, and (c) coal specimen.

The axial, radial, and volumetric strains are all greater postfracture than prefracture. The stress-strain curves can be divided into three stages corresponding to elastic, plastic, and fracture strain. The axial strain decreases obviously as the confining pressure increases from 4 to 6 to 8 MPa in the elastic strain stage, while the radial and volumetric strains are almost unchanged. In contrast, the axial, radial, and volumetric strains all decrease clearly in the plastic strain stage, and the strain values of axial strain ε_1, radial strain ε_3, and volumetric strain ε_v increase at the rupture site. After exceeding the stress peak of the specimen, coal inner microcracks begin to extend, and to be further interfingering, block coal is broken into smaller coal fragments by crack network. Axial stress starts to fall down suddenly, porosity becomes larger, and residual stress of cracked coal maybe exceeding coal strength results in coal recrack continuously. All of the strains suddenly and substantially increase during the postfracture stage.

Therefore, the stresses, including the axial stress σ_1 and confining pressure σ_3, and pore pressure p more significantly affect coal in the elastic and plastic strain stages than in the fracture strain stage.

As shown in Figure 4, at a confining pressure of 6 MPa, the compression strength of the coal specimen decreases rapidly as the pore pressure changes from 1 to 2 MPa; however, the axial and radial strains increase slowly at the same confining pressure, and the strain oscillation diminishes in the fracture stage. The adsorption capacity of the anthracite increases gradually with increasing pore pressure, and the adhesion between coal particles decreases due to the increased adsorption-induced swelling deformation. Although the pore pressure can offset part of the axial stress, the adsorbed layer caused by the swelling deformation results in lubrication during the fracturing process and evidently reduces the coal strength. The research results were basically similar as those of other scholars.

The linear increases of the elastic modulus E and compression strength σ_c with increasing confining pressure are depicted in Figure 5. The inner pores and cracks of the coal specimen are restricted to expand in the radial direction

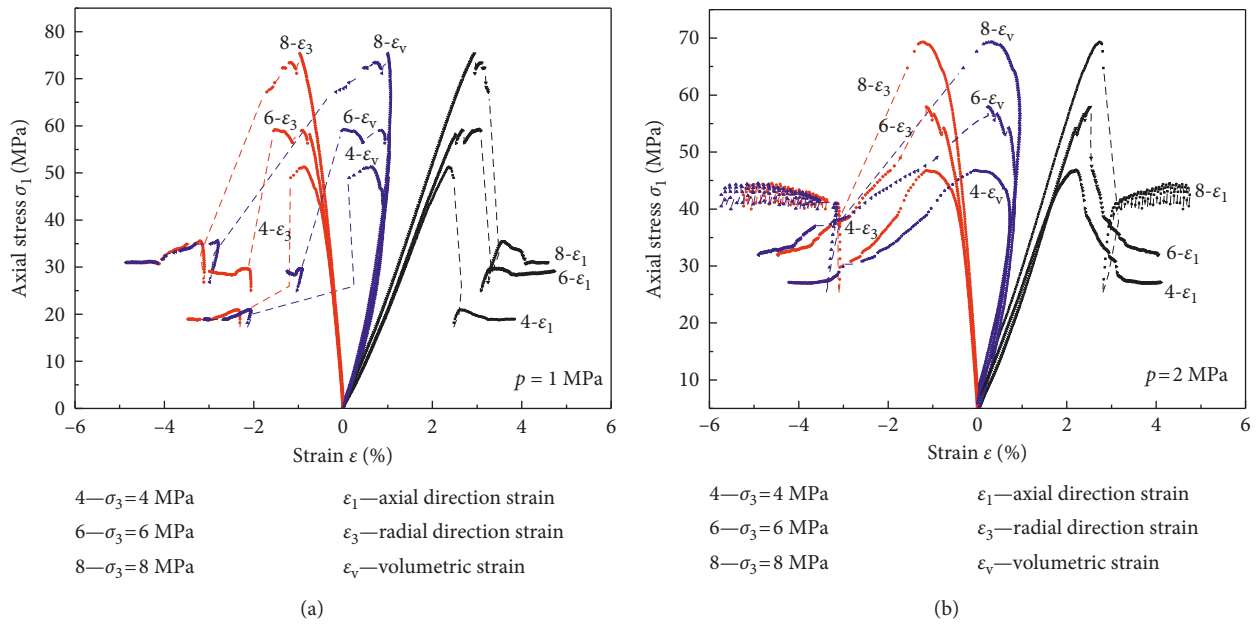

Figure 3: Relationship between axial stress and strain at pore pressures of (a) 1 MPa and (b) 2 MPa.

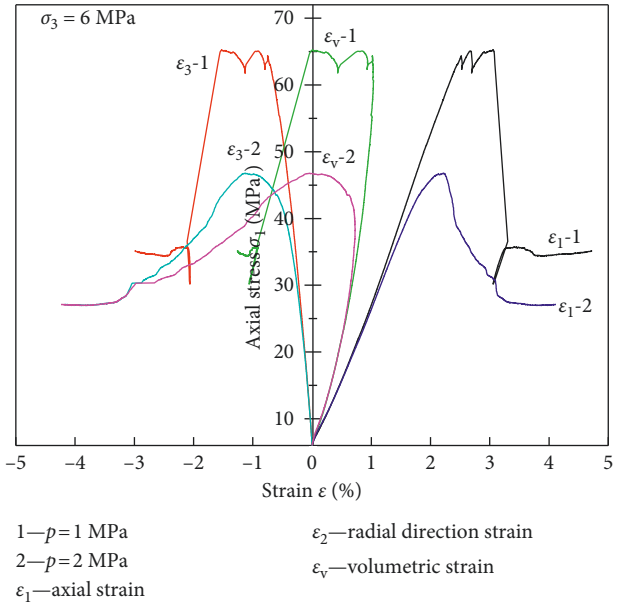

Figure 4: Relationship between stress and strain at different pore pressures.

under the confining pressure, and the pore and crack volume is compressed further under the axial pressure, causing the friction between the coal particles to increase.

3.2. Deformation Effects on Permeability. The authentic stress state of coal can be expressed in terms of the average effective stress according to the Terzaghi formula [27–29] since the effective stress is one of the primary factors affecting the coal strength, deformation, and permeability. The formula is as follows:

$$\begin{aligned}\sigma_1' &= \sigma_1 - p_1,\\ \sigma_3' &= \sigma_3 - \frac{1}{2}(p_1 + p_2),\\ \sigma_0 &= \frac{1}{3}(\sigma_1 + 2\sigma_3) - \frac{1}{2}(p_1 - p_2),\end{aligned} \tag{2}$$

where σ_1 denotes the axial stress, MPa; σ_1' is the effective axial stress, MPa; σ_3 represents the confining pressure, MPa; σ_3' is the effective confining pressure, MPa; σ_0 denotes the average effective stress, MPa; and p_1 and p_2 demote gas inlet and outlet pressures, respectively, MPa.

Using the Terzaghi formula, the effective stress of the coal specimen was calculated for different axial stresses and pore pressures, as shown Table 2.

Based on the results, a curve illustrating permeability changes with axial strain and pore pressure was drawn (Figure 6). It reveals the correlation between permeability and effective stress σ_0 and between permeability and axial strain, at different pore pressures and a confining pressure of 6 MPa.

With increasing axial strain, the seepage velocity exhibits a parabolic shape first decreasing and then increasing, while the effective stress increases linearly in the initial elastic deformation stage. With increasing pore pressure, the seepage velocity decreases rapidly in the initial compressed stage and then increases slowly at a constant confining pressure of 6 MPa. The effective stress-strain curves at pore pressures of 1 MPa and 2 MPa are the same in the lower strain stages ($\varepsilon_1 < 1.5\%$), while that corresponding to a pore pressure of 2 MPa is larger in the higher strain stages ($\varepsilon_1 > 1.5\%$). However, the decrease rate of permeability curves are the same in the lower strain stages ($\varepsilon < 1.5\%$) at p = 1MPa and p = 2MPa, and they at p = 1MPa increase

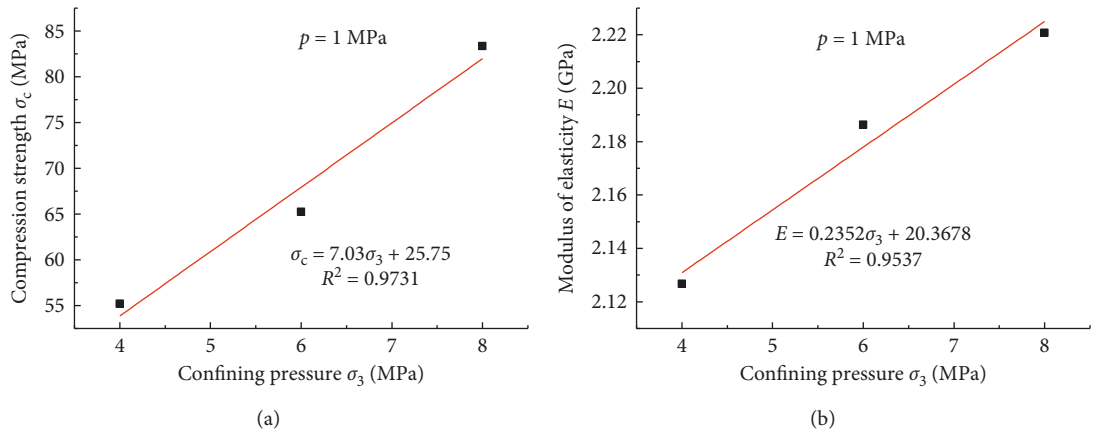

Figure 5: Variations of (a) compression strength and (b) modulus of elasticity with confining pressure.

Table 2: Test parameters of average effective stress-seepage velocity.

Specimen no.	Gas pressure (MPa)	Average effective stress, $\sigma_{0,max}$		Residual effective stress, σ_r	
		σ_0 (MPa)	q_{max} (mL/min)	σ_r (MPa)	q_{max} (mL/min)
W1		20.60	0.384	9.78	1.512
W2	1	25.19	0.032	15.16	0.035
W3		32.56	0.030	17.77	0.034
W4		20.91	0.577	12.29	3.496
W5	2	18.54	0.015	11.98	0.132
W6		27.38	0.161	18.44	0.274

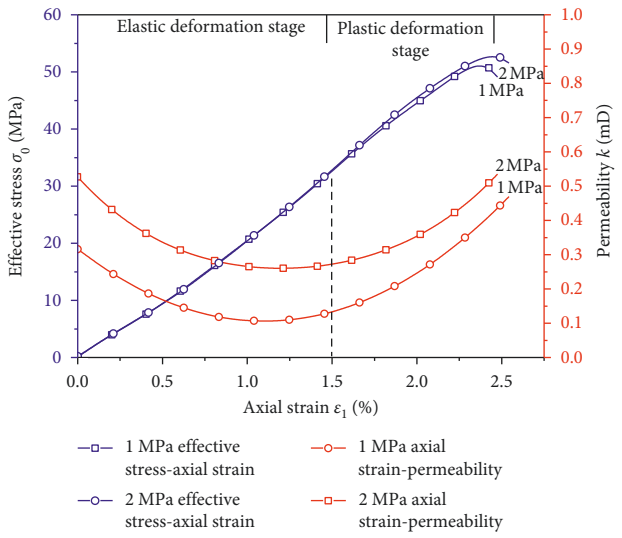

Figure 6: Relationships between effective stress, permeability, and axial strain at a confining pressure of 6 MPa.

more rapidly than those at 2 MPa in the higher strain stages ($\varepsilon_1 > 1.5\%$). Compared with other scholars, the change of permeability and strain is different. The main reasons are that testing specimens have lower porosity, abundant nanostructure pores, and strong absorbable behavior. Absorption inducing swelling strain of specimen is smaller, and the permeability is larger at low pore pressure.

Therefore, the coal permeability decreases in the law of negative exponent function as the increases in the law of exponential function as the increase of effective stress in the plastic stage. The difference between the effective stress curves is barely observable in the elastic strain stage, although it is obvious in the plastic strain stage. From the comparison, it can be found that gas is easier to flow in the plastic deformation stage than in the elastic deformation stage. The difference between the permeability curves is clear since that corresponding to the greater pore pressure is obviously higher, and the initial difference between the permeability curves is larger than it is after the application of a greater axial strain.

3.3. Time Effects on Permeability. Coal is a dual-pore-system medium, containing matrix and fissure-pore systems of different sizes. The permeability of coal mainly depends on the fissures, which not only provides gas reservoir space but also connects the matrix pores via a microfissure network system. As shown in Figure 7, as the confining pressure increases from 4 to 8 MPa, the maximum average effective stress $\sigma_{0,max}$ increases linearly from 20.6 to 32.56 MPa during the prefracture stage and decreases rapidly during the postfracture stage. However, the residual stress increases from 9.78 to 15.16 MPa and finally to 17.77 MPa. The fracturing frequency of the coal increases obviously in the fracture stage with increasing confining pressure. The effective stress curves exhibit serrated changes due to the

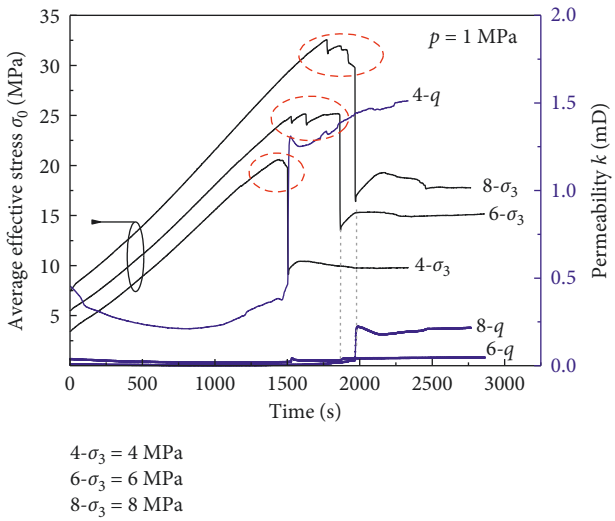

FIGURE 7: Time dependences of average effective stress and permeability.

stretch of microcracks and interconnection inside the coal body, as the increasingly numerous microcracks become larger cracks and form cracks. Finally, the coal specimen is broken, resulting in an exponential increase in permeability.

At a constant confining pressure, the permeability first rapidly decreases, then slightly increases, rapidly increases, and becomes relatively stable. Different confining pressures yield different permeability and dissimilar rates of decrease and increase. The rates of change decrease with increasing effective stress.

The time from compression until the first break in the coal specimen is approximately 1500 s, 1700 s, and 1900 s at confining pressures of 4 MPa, 6 MPa, and 8 MPa, respectively. These times reflect the inverse relationship between the coal methane seepage velocity and effective stress. The greater the confining pressure is, the higher the yield strength is, and the higher the compressive strength is, the longer the time from a quantitative change until a qualitative change is.

3.4. Temperature Effects on Permeability. The permeability experimentally obtained at different temperatures and pore pressures of 2 MPa is presented in Figure 8. The initial permeability decreases almost linearly with increasing temperature, and its rate of decrease continuously decreases as the temperature increases further (Figure 8(a)). The variations of the minimum permeability with temperature are similar to those of the initial permeability; however, the rate of change of the minimum permeability decreases more slowly than that of the initial permeability as the confining pressure increases (Figure 8(b)). The maximum permeability exhibits the same tendency to decrease as the confining pressure increases from 4 MPa to 6 MPa to 8 MPa (Figure 8(c)).

These changes indicate that temperature significantly affects permeability, which displays an inverse relationship with temperature. The initial and the minimum permeability of the specimen decrease 53% and 7.2% as temperature increases from 30°C to 50°C. The initial permeability is greater than the minimum permeability at different temperatures, while the sensitivity decreases with increasing temperature.

In general, the observed effects of temperature on permeability are complex. First, when the thermal stress was less than the external stress, volume expansion and thermal stress were produced as the temperature increased, causing inward expansion that compressed the pores and decreased the permeability, and the differences between the porosity and permeability curves increased. Then, the coal adsorption capacity increased, and the adsorbed methane began to desorb with increasing temperature, causing the coal matrix to shrink and the effective porosity to increase, resulting in increased permeability. Finally, the methane molecule preserved coal pores, and cracks enabled more rapid and easier flow under the same external stress with increasing temperature. Thus, the permeability is more sensitive to stress than temperature in coal reservoirs.

Temperature takes an important influence on mechanic's characteristic, methane adsorption/desorption, and methane seepage of coal containing gas. There is no a uniform viewpoint, and still many contest about temperature is how to effect the permeability according to the different experimental results. Some scholars believed that permeability increase with the increasing temperature, and also others insisted in the reverse opinion.

As shown in Figure 9, when temperature changes from 30°C to 40°C to 50°C, the elastic modulus of coal containing gas increases to 12.9% and 5.97% and compression strength decreases to 9.7% and 17.6%, respectively. Analyzing the tendency towards change, it is believed that coal adsorption capacity became larger and methane molecules moved faster under thermal motion to produce larger gas internal energy. This further weakened mechanics characteristic of coal containing gas. The conclusion is basically in consonance with other studies on different rank coal and modeled coal.

4. Conclusions

Six deformation-seepage tests under different stress confining conditions and temperatures were conducted. Gas seepage effect and efficiency were evaluated and discussed from different aspects. The research progress can be considered for improving the gas-drainage efficiency in underground colliery or in CBM field especially in low-permeability high gas seams. In the further research, permeability and strain of different tectonically deformed coals should be adapted to improve and perfect the theory of CBM:

(1) Pore pressure, temperature, and confining pressure significantly influence the formation and permeability of coal containing gas. At a constant confining pressure and temperature, the permeability of coal methane increases linearly with increasing pore pressure. However, the permeability has a parabolic

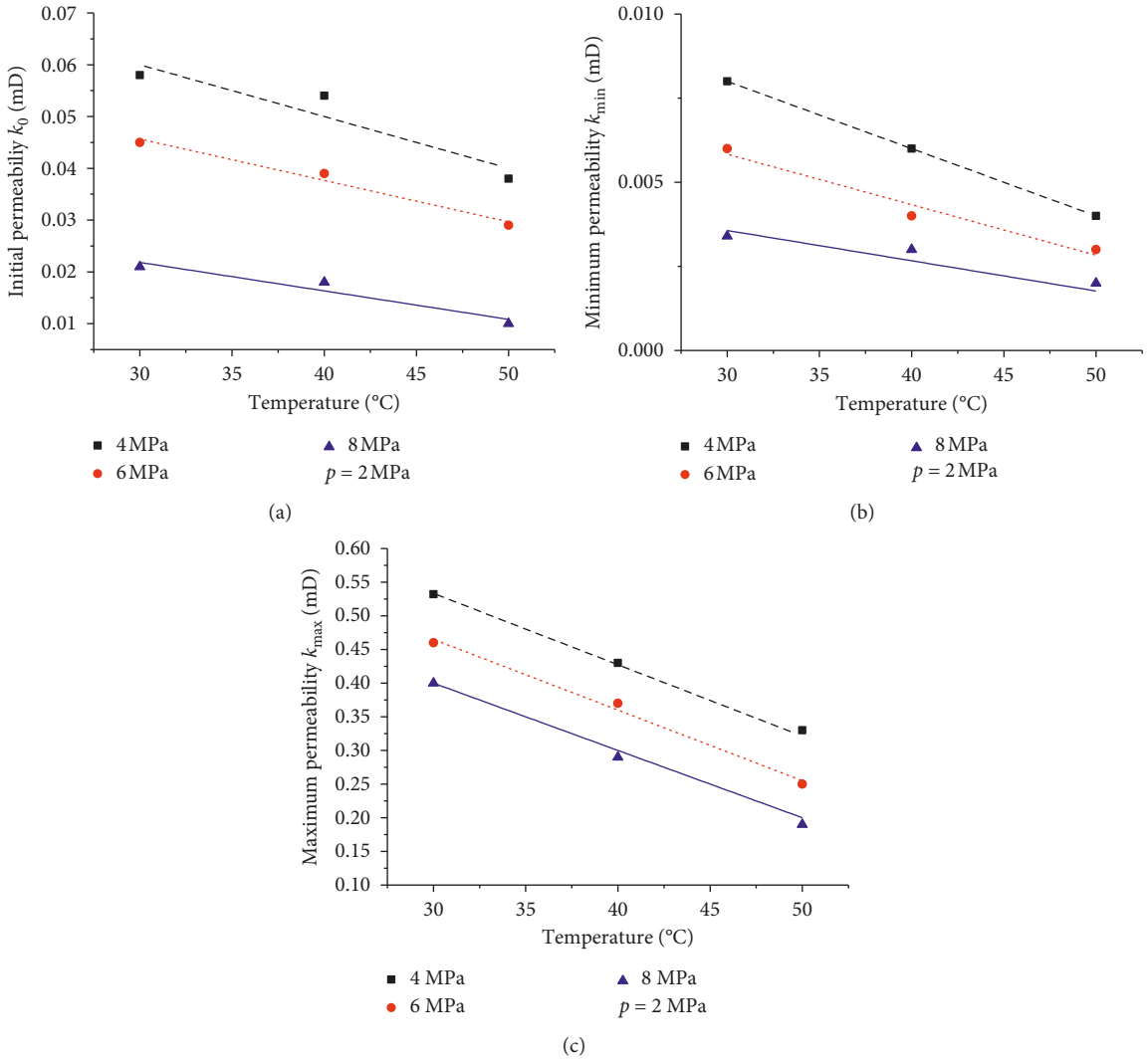

Figure 8: Relationships between (a) initial, (b) minimum, and (c) maximum permeability and temperature at different confining pressures.

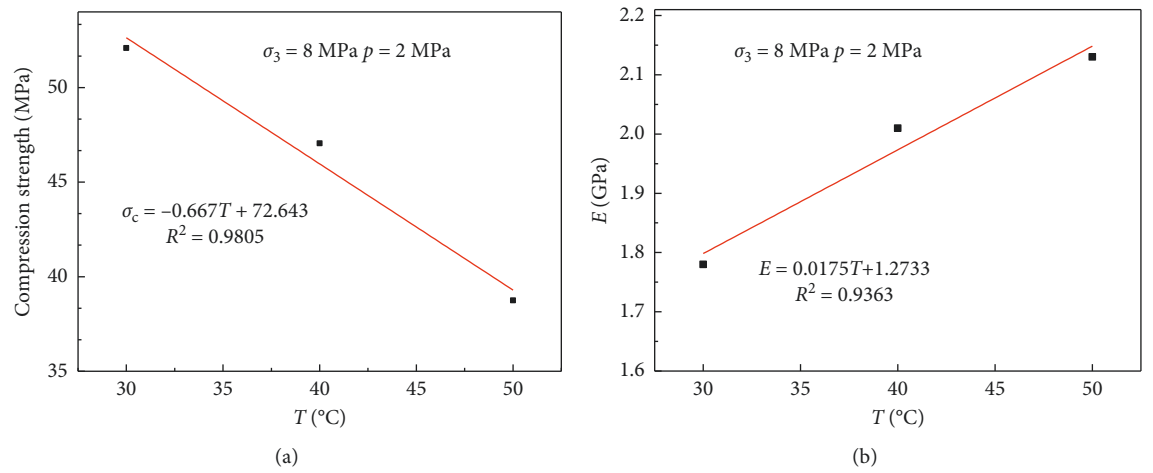

Figure 9: Relation between (a) compression strength and temperature and between (b) elastic modulus and temperature at a confining pressure of 8 MPa and pore pressure of 2 MPa.

relationship with the confining pressure, first decreasing rapidly and then increasing slowly, and the initial permeability, minimum permeability, and maximum permeability (from 0.532, 0.46, 0.4 to 0.33, 0.25, to 0.19) all change obviously.

(2) As the axial stress increases, the axial and radial strains and compression strength increase, but the compression strength and strain decrease clearly as the pore pressure increases from 1 MPa to 2 MPa.

(3) Effective stress controls the dynamic changes of permeability in low-strain stage ($\varepsilon_1 < 1.5\%$), yet pore pressure decides its changes in larger strain stage ($\varepsilon_1 > 1.5\%$). At the same temperature and in the low-strain stages, the effective stress increases linearly as the axial strain increases. In contrast, the permeability first decreases rapidly and then increases slowly. As the confining pressure continues to increase, the effective stress increases further and the permeability reaches its minimum. The permeability subsequently begins to increase, as do the fracturing time and number of fractures. With increasing temperature, the initial permeability decreases obviously. Meanwhile, the minimum permeability generally becomes more consistent as the confining pressure increases, although slight changes with temperature may still be observed.

(4) The variation of permeability induced by effective stress is greater and more sensitive than that by temperature in gas production process.

Data Availability

The data used to support the findings of this study are available from the corresponding author upon request.

Conflicts of Interest

The authors declare that they have no conflicts of interest.

Acknowledgments

This work was financially supported by the National Natural Science Foundation of China (Grant no. 41572139), the doctoral foundation of Henan Polytechnic University (B2015-79), and the Innovative Research Team (in Science and Technology) in the University of Henan Province (17IRTSTHN025). The authors also thank the technical staff in UOW and HPU. The authors would like to thank Editage (http://www.editage.cn) for English language editing.

References

[1] J. Lin, T. Ren, G. Wang, P. Booth, and J. Nemcik, "Experimental investigation of N_2 injection to enhance gas drainage in CO_2-rich low permeable seam," *Fuel*, vol. 215, pp. 665–674, 2018.

[2] J. Enever and A. Hennig, "The relationship between permeability and effective stress for Australian coals and its implications with respect to coalbed methane exploration and reservoir modelling," in *Proceedings of 1997 International Coalbed Methane Symposium*, Tuscaloosa, AL, USA, May 1997.

[3] Y. Li, D. Tang, H. Xu, Y. Meng, and J. Li, "Experimental research on coal permeability: the roles of effective stress and gas slippage," *Journal of Natural Gas Science and Engineering*, vol. 21, pp. 481–488, 2014.

[4] Y. Meng, Z. Li, and F. Lai, "Experimental study on porosity and permeability of anthracite coal under different stresses," *Journal of Petroleum Science and Engineering*, vol. 133, pp. 810–817, 2015.

[5] Z. Meng and G. Li, "Experimental research on the permeability of high-rank coal under a varying stress and its influencing factors," *Engineering Geology*, vol. 162, pp. 108–117, 2013.

[6] D. Wang, J. Wei, and G. Yin, "Investigation on change rule of permeability of coal containing gas under complex stress paths," *Chinese Journal of Rock Mechanics and Engineering*, vol. 31, no. 2, pp. 303–310, 2012.

[7] S. Wu, D. Tang, S. Li, H. Wu, X. Hu, and X. Zhu, "Effects of geological pressure and temperature on permeability behaviors of middle-low volatile bituminous coals in eastern Ordos Basin, China," *Journal of Petroleum Science and Engineering*, vol. 153, pp. 372–384, 2017.

[8] L. D. Connell, "A new interpretation of the response of coal permeability to changes in pore pressure, stress and matrix shrinkage," *International Journal of Coal Geology*, vol. 162, pp. 169–182, 2016.

[9] X. Jiang, C. Jie, and L. Bobo, "Experimental research on response law of permeability of coal to pore pressure," *Chinese Journal of Rock Mechanics and Engineering*, vol. 32, no. 2, pp. 225–230, 2013.

[10] G. Yin, C. Jiang, J. Wang, and J. Xu, "Combined effect of stress, pore pressure and temperature on methane permeability in anthracite coal: an experimental study," *Transport in Porous Media*, vol. 100, no. 1, pp. 1–16, 2013.

[11] Y. Tao, J. Xu, S. Peng, and M. Yuan, "Experimental study of influencing factor of porosity and effective stress of gas-filled coal," *Rock and Soil Mechanics*, vol. 31, no. 11, pp. 3417–3422, 2010.

[12] P. Guo, Y. Cheng, K. Jin, W. Li, Q. Tu, and H. Liu, "Impact of effective stress and matrix deformation on the coal fracture permeability," *Transport in Porous Media*, vol. 103, no. 1, pp. 99–115, 2014.

[13] S. Harpalani and G. Chen, "Influence of gas production induced volumetric strain on permeability of coal," *Geotechnical and Geological Engineering*, vol. 15, no. 4, pp. 303–325, 1997.

[14] R. Lu, S. Peng, G. Liu, B. Li, J. Pan, and X. Lin, "High-pressure methane adsorption-induced coal swelling on equilibrium moisture coal samples," *Energy Sources Part A: Recovery Utilization and Environmental Effects*, vol. 38, no. 14, pp. 2119–2127, 2016.

[15] G. Wang, X. Wei, K. Wang, P. Massarotto, and V. Rudolph, "Sorption-induced swelling/shrinkage and permeability of coal under stressed adsorption/desorption conditions," *International Journal of Coal Geology*, vol. 83, no. 1, pp. 46–54, 2010.

[16] W. Zhu, C. Wei, J. Liu, T. Xu, and D. Elsworth, "Impact of gas adsorption induced coal matrix damage on the evolution of coal permeability," *Rock Mechanics and Rock Engineering*, vol. 46, no. 6, pp. 1353–1366, 2013.

[17] L. D. Connell, M. Lu, and Z. Pan, "An analytical coal permeability model for tri-axial strain and stress conditions," *International Journal of Coal Geology*, vol. 84, no. 2, pp. 103–114, 2010.

[18] Z. Fang, X. Li, and L. Huang, "Laboratory measurement and modelling of coal permeability with different gases adsorption," *International Journal of Oil, Gas and Coal Technology*, vol. 6, no. 5, pp. 567–580, 2013.

[19] J.-Q. Shi, S. Durucan, and S. Shimada, "How gas adsorption and swelling affects permeability of coal: a new modelling approach for analysing laboratory test data," *International Journal of Coal Geology*, vol. 128-129, pp. 134–142, 2014.

[20] G. Yin, C. Jiang, X. Li, W. Wang, and B. Cai, "An experimental study of gas permeabilities of outburst and nonoutburst coals under complete stress-strain process," *Rock and Soil Mechanics*, vol. 32, no. 6, pp. 1613–1619, 2011.

[21] J. Zou, W. Chen, D. Yang, H. Yu, and J. Yuan, "The impact of effective stress and gas slippage on coal permeability under cyclic loading," *Journal of Natural Gas Science and Engineering*, vol. 31, pp. 236–248, 2016.

[22] S. Liu and S. Harpalani, "Determination of the effective stress law for deformation in coalbed methane reservoirs," *Rock Mechanics and Rock Engineering*, vol. 47, no. 5, pp. 1809–1820, 2014.

[23] Z. Pan, L. D. Connell, and M. Camilleri, "Laboratory characterisation of coal reservoir permeability for primary and enhanced coalbed methane recovery," *International Journal of Coal Geology*, vol. 82, no. 3-4, pp. 252–261, 2010.

[24] R. Chen, Y. Qin, P. Zhang, and Y. Wang, "Changes in pore structure of coal caused by CS2 treatment and its methane adsorption response," *Geofluids*, vol. 2018, Article ID 7578967, 11 pages, 2018.

[25] Z. Shining, "Mechanism of gas flow in coal seams," *Journal of China Coal Society*, vol. 15, no. 1, pp. 15–24, 1990.

[26] H. Zhang, J. Liu, and D. Elsworth, "How sorption-induced matrix deformation affects gas flow in coal seams: a new FE model," *International Journal of Rock Mechanics and Mining Sciences*, vol. 45, no. 8, pp. 1226–1236, 2008.

[27] M. He, C. Wang, D. Li, J. Liu, and X. Zhang, "Desorption characteristics of adsorbed gas in coal samples under coupling temperature and uniaxial compression," *Chinese Journal of Rock Mechanics and Engineering*, vol. 29, no. 5, pp. 865–872, 2010.

[28] X. Yang, Y. Zhang, C. Li, and W. Li, "Experimental study on desorption and seepage rules of coal-bed gas considering temperature conditions," *Chinese Journal of Geotechnical Engineering*, vol. 30, no. 12, pp. 1811–1814, 2008.

[29] R. Lv, B. Li, Z. Song, G. Liu, and J. Ren, "Deformation and seepage mechanical model for loaded gas-bearing coal masses," *Journal of Computational and Theoretical Nanoscience*, vol. 13, no. 9, pp. 6365–6371, 2016.